Hindawi
Geofluids
Volume 2022, Article ID 1692516, 20 pages
https://doi.org/10.1155/2022/1692516

Research Article

Factors Influencing the Pore Structure and Gas-Bearing Characteristics of Shales: Insights from the Longmaxi Formation, Southern Sichuan Basin and Northern Yunnan-Guizhou Depression, China

Li Dong,[1] Changcheng Han ,[2,3] M. Santosh,[4] Yongkai Qiu,[4] Geng Liu,[2] Jinghui Ma,[2,3] Hao He,[5] and Chenlin Hu[2,3]

[1]*Petroleum Exploration and Production Research Institute, Sinopec, Beijing 102206, China*
[2]*College of Geology and Mining Engineering, Xinjiang University, Urumqi 830047, China*
[3]*Xinjiang Key Laboratory for Geodynamic Processes and Metallogenic Prognosis of the Central Asian Orogenic Belt, Urumqi 830047, China*
[4]*School of Earth Sciences and Resources, China University of Geosciences Beijing, 29 Xueyuan Road, Beijing 100083, China*
[5]*Petroleum Exploration and Development Institute, Tarim Oilfield Company, PetroChina, Korla 841000, China*

Correspondence should be addressed to Changcheng Han; hanchangchen@126.com

Received 2 March 2022; Accepted 6 May 2022; Published 6 June 2022

Academic Editor: Dazhong Ren

China hosts rich shale gas resources. The Longmaxi Formation (LF) in the Sichuan Basin is one of the important regions for shale gas exploration and extraction. Here, we investigate the pore structure and factors influencing the gas-bearing characteristics of the pores in the shale reservoirs in the LF. We employed scanning electron microscopy (SEM), X-ray diffraction analysis (XRD), gas content testing, gas saturation testing based on nuclear magnetic resonance (NMR), overburden porosity and permeability analysis, distribution of pore size, specific surface area (SSA) analysis, and geochemical analysis. Our results show that the organic matter of the shale in the LF in the study area is highly favorable to shale gas conditions; the brittleness of the regional shale generally increases with an increase in depth. The pores in the LF mainly include organic matter-hosted pores, intergranular pores, intragranular pores, and microfissures, with mesopores dominating. Meanwhile, the gas content also increases with an increase in depth. The pore structure in the study area is affected by organic matter content and mineral components, with the development of organic matter-hosted pores. The porosity and the SSA are positively correlated with the total organic carbon (TOC), whereas clay minerals have an adverse effect on the SSA of pores in the study area. Higher TOC and vitrinite reflectance (Ro) indicate higher gas content. It can be inferred that as the content of brittle minerals increases, particles break to form storage spaces as the depth increases, causing the gas content to increase. Higher SSA and total pore volume indicate higher volume of adsorbed gas. The bound water in rocks tends to reduce the content of desorbed gas. Our results suggest high potential for shale gas extraction in this region.

1. Introduction

Shale gas refers to natural gas mined from dark or organic matter-rich shale. It self-generates, self-stores, and continuously accumulates in nanoscale shale pores, where it occurs on the surfaces of organic matter and clay minerals in the form of absorbed gas or in micro-nano pores of organic matter shale in the form of free gas [1–6]. Shale gas is formed due to biogenic or thermogenic origin over time [7]. In recent years, shale gas has become an important part of oil and gas production, as represented by the shale gas revolution in the United States [8, 9]. Shale gas reserves have also contributed critically to the increases in global oil and gas reserves [10, 11]. China enjoys very rich shale gas resources

[12, 13]. The LF in the Sichuan Basin is one of the country's critical horizons for shale gas exploration and extraction [14–17]. Given the increasing commercial interests in shale gas, several recent studies have focused on shale gas reservoirs [18–21]. In general, shale reservoirs have low porosity, low permeability, and extremely uneven pore structure [22–25]. Pore structure plays a certain role in determining the preservation and enrichment of shale gas in deep reservoirs [26]. Specifically, it has significant impacts on the occurrence, migration, and enrichment of natural gas [27–29]. The gas-bearing characteristics of the pores also affect the extractability. Meanwhile, the gas content is a vital parameter determining the reserves of shale gas reservoirs [30, 31], and high gas content is critical for successful shale exploitation [32].

In this study, we investigate the nature and role of pore structure and GBP of shale in the LF and their influencing factors. We carried out overburden porosity and permeability analysis, whole rock analysis, geochemical analysis, gas content testing, and pore microscopic analysis. Our results provide potential scope for shale gas exploration in this region and also provide a reference base for the exploration and extraction of oil and gas reservoirs in similar occurrences elsewhere.

2. General Geology and Sample Sources

The study of the LF is located in the southern part of the Sichuan Basin and the northern part of the Yunnan-Guizhou Depression (Figure 1(a)). The LF comprises very thick and well-preserved shale and is a key horizon for shale gas exploration. Shale samples were taken from eight wells drilled in the study area (Figure 2).

3. Samples and Methodology

This study used samples of LF shale taken from eight wells in the study area.

3.1. XRD Analysis. We employed RINT-TTR3X-ray diffractometer to authenticate and analyze the mineral components of samples. Fifty-six shale samples were selected from six wells and ground to 200 mesh. Mineral powder and clay powder were separated from each other and dried before analysis. Since different minerals have different characteristics, the content of a mineral can be determined by the intensity of the characteristic peaks of the mineral.

3.2. Measurement of Porosity and Permeability. A Coreval 700 overburden porosity-permeability instrument supplied by VINCI, France was employed to determine the porosity and permeability of each of the 48 shale samples taken from different wells. The porosity and permeability are used to characterize the physical characteristics of pores. Core column samples with a length of 3 cm were clamped using clampers and connected to the control center of the Coreval 700 instrument. Then, different overburden and confining pressures were applied to the samples from different wells. The permeability was measured using pressure pulse attenuation. Specifically, pressure was exerted on the core, and then, the pressure differential between both ends of a sample was measured. Employing the principle of Boyle's Law, the porosity was calculated by solving the equation of the gas state according to a known volume and the pressure changes obtained by helium expansion.

3.3. Scanning Electron Microscopy (SEM) Observation. Pore structure and minerals were analyzed on a micro-nano scale using a ZEISS electronic microscope. Samples were taken at different depths of well L1 and cut into pieces of about 1 cm^3. These pieces were then ground and polished with argon ions to remove ragged surfaces and matters attached to their surfaces. Then, the samples were installed using carbon-coated resin to improve the quality of high-resolution imaging. Both secondary and back-scattered electronic images were obtained and used to study the characteristics of the pore structure.

3.4. Measurement of Specific Surface Area (SSA) and Pore Size. The pore size, SSA, and total pore volume of 56 shale samples were measured using a Micromeritics ASAP2420 specific-surface-area tester. The tester uses helium and nitrogen as adsorbents, and the steps are as follows. A total of 500 mg shale samples were taken and ground to below 60 meshes. These were vacuumized for 3 h at the vacuum level of 1×10^{-3} Pa and then placed at 120°C for 24 h to remove any moisture and volatiles in the samples. The samples were then analyzed using the surface analysis system to obtain the pore size and the SSA. The measurement range of SSA, pore volume, and pore size were 0.0005–5000 m^2/g, <0.0001 cc/g, and 0.35–500 nm, respectively.

3.5. Geochemical Analysis. The TOC of 105 shale samples was measured in accordance with GB/T 19145-2003 using a Leco C-S determinator. During this process, the Ca and S in the samples were oxidized and to turn into the gases CO_2 and SO_2 after the samples were heated at a high temperature (1000°C) for 2 h in an O2-rich condition. The gas was introduced into corresponding adsorption cells to adsorb IR radiation, during which signals were produced using a detector. The signals were processed by a computer to obtain results. The TOC in measured results was used in this study. Using a J&M PMT IV photometer, the maturity of the organic matter in 18 shale samples was measured as per Chinese standard SY/T5124-1995 *Determination of Vitrinite Reflectance in Sedimentary Rock*. Spectrophotometers generated light sources with various wavelengths and a series of light-splitting devices helped to produce a light source with certain wavelengths. Samples absorbed specific lights after being exposed to the light source. The anthraxolite reflectivity (*Rb*) was measured at an ambient temperature of 23 ± 3°C, relative humidity (RH) of <70%, a measuring wavelength of 546 nm, microscope magnification of 125 multiples, reflectivity range of 0.1%–10.0%, and resolution of 0.01%. Next, the equivalent vitrinite reflectivity *Ro* was obtained through conversion using equation $Ro' = 0.3364 + 0.6569 \times Rb$. Kerogen types were observed under a Leica DM4500P microscope. The type of organic matter in each sample can be distinguished under a fluorescence

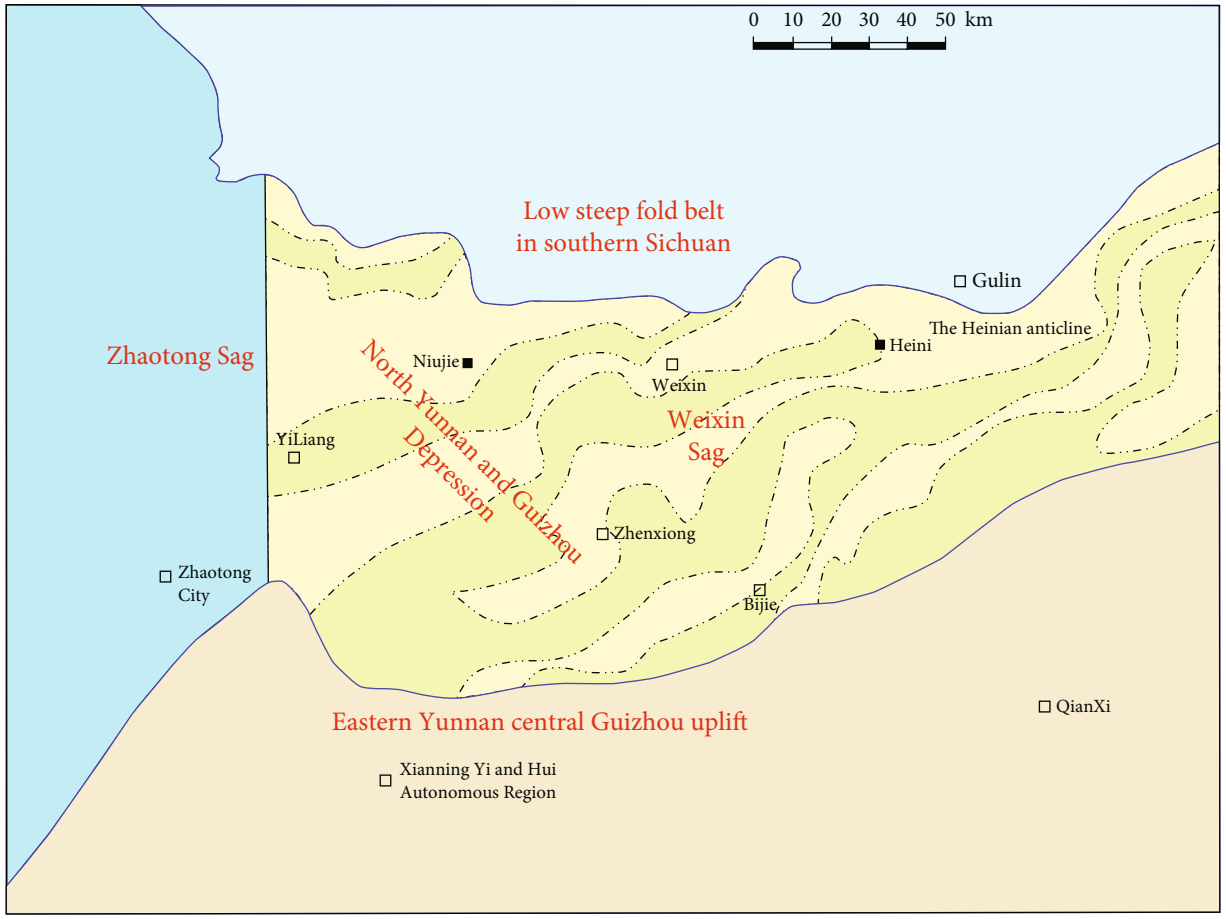

(a)

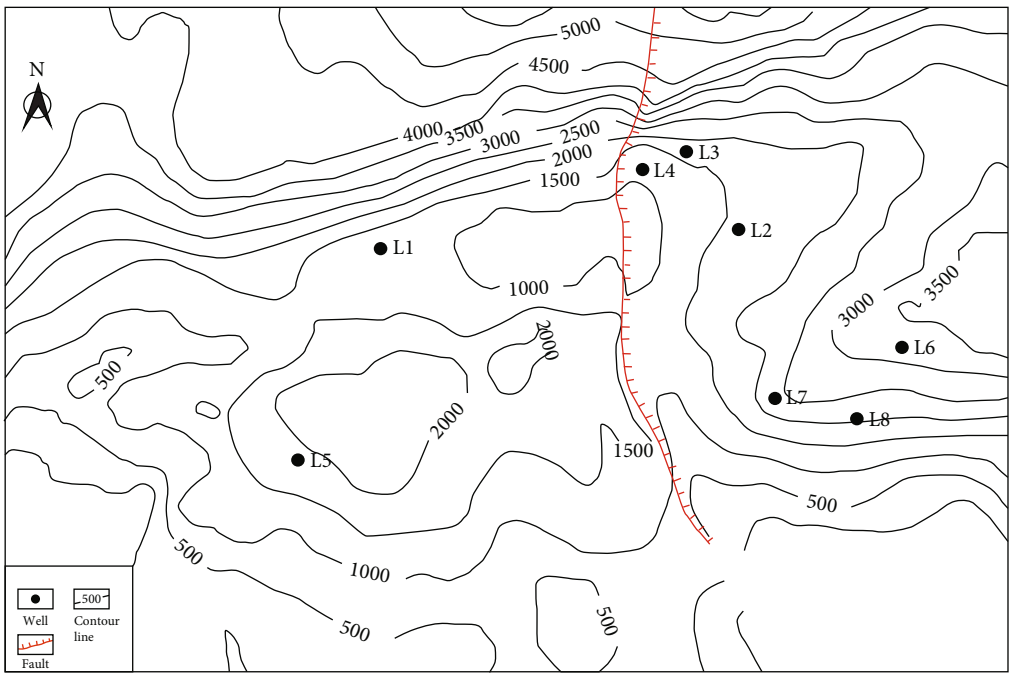

(b)

Figure 1: Maps showing the location of the study area. (a) The sketch map showing the Sichuan Basin and its adjacent area. (b) The map showing the wells distribution, contour line, and faults of the study area.

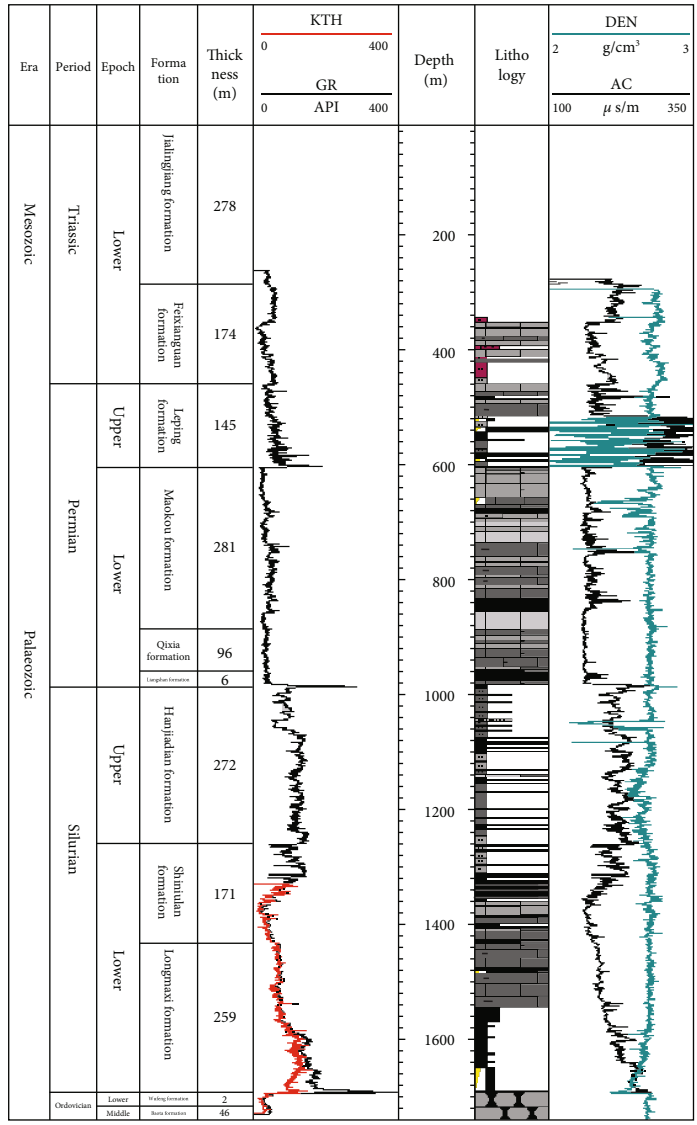

Figure 2: Lithofacies of a single well.

microscope. For example, shiny, yellow, and amorphous particles are saprolites, whereas fibrous or virgate particles that are not luminous are humus. In this way, the types of organic matter in the study can be determined.

3.6. Gas Content. The gas content of 56 core samples was measured using the desorption method at the coring sites during well drilling. Once taken out of the well, the cores were immediately placed in a desorption tank, where they were naturally desorbed under simulated stratigraphic temperature to determine the content of the desorbed gas. The volume of the lost gas was obtained through linear regression using the USBM method [33]. In the initial stage of equilibrium diffusion, the core is separated from the reservoir for a short time, and the core temperature does not change significantly. In this stage, the gas diffusion coefficient basically remains constant, and the original total gas volume and characteristic diffusion distance of the same core remain unchanged. Thus, the

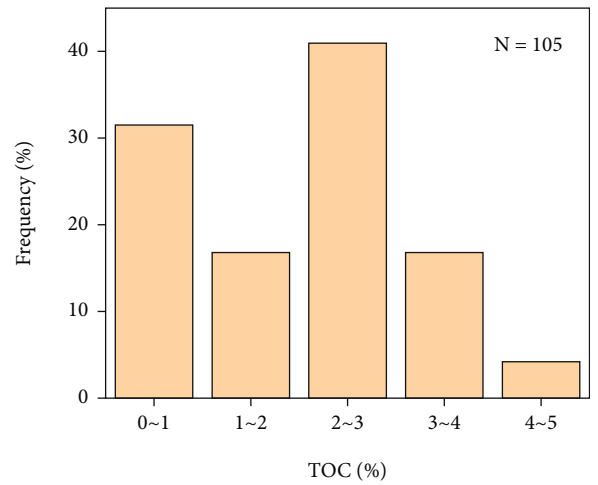

Figure 3: Histogram showing the TOC of the LF in the study area.

Table 1: TOC, *Ro*, and organic matter types of the LF in the study area.

SampleNo.	TOC (%)	Ro (%)	Organic matter type	Sample No.	TOC (%)	Ro (%)	Organic matter type
L1-7	1.10	2.15	II_2	L3-8	3.35	2.26	II_1
L1-14	2.60	/	/	L3-10	3.50	/	/
L1-17	2.70	2.11	II_2	L3-11	4.28	2.54	II_1
L1-20	3.10	/	/	L4-1	/	2.08	II_1
L1-23	3.50	2.24	II_2	L4-4	/	2.21	II_1
L2-3	2.00	/	/	L4-10	/	2.36	II_1
L2-5	2.40	/	/	L4-16	/	2.02	II_1
L2-7	2.40	2.53	/	L4-19	/	2.17	II_1
L2-8	2.50	/	/	L5-1	0.84	/	II_1
L2-14	4.20	2.71	/	L5-9	0.56	/	II_1
L3-2	2.30	/	/	L5-15	1.93	/	/
L3-3	2.57	2.20	II_1	L5-21	3.42	/	II_1

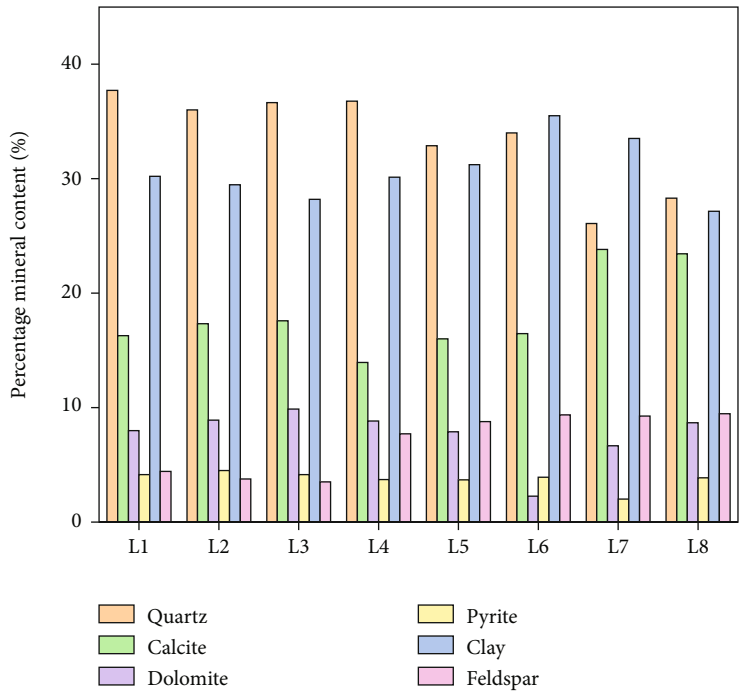

Figure 4: Histogram showing the content distribution of the LF minerals in wells in the study area.

accumulated desorption gas collected at this stage has a linear relationship with the square root of diffusion time, and the lost gas can be obtained by extrapolating its linear trend line to the zero time point.

3.7. Adsorbed Gas Volume. The volume of adsorbed shale gas in 10 samples from well L2 was measured using a high-pressure isothermal adsorption instrument Rubertherm ISOSORP-HP Static. A magnetic suspension balance was used to directly measure the changes in the weight of each sample in the process of adsorption/desorption and to immediately obtain the samples' adsorption/desorption volume. Based on the temperature and pressure conditions in the strata where samples were taken, the temperature was set to 60°C, the initial pressure was set to 0 MPa, and the upper threshold was set to 30 MPa. The volume of adsorbed gas was then measured at 60°C and under different pressures. The Langmuir adsorption model assumes that shale solids with even and smooth surfaces form monolayer adsorption and that there is no interaction force between molecules of adsorbed gas. After the volume of adsorbed gas was measured, the volume of adsorbed gas was calculated through fitting using the Langmuir equation $Vex = V_L * P/(P_L + P) * (1\text{-}\rho_g/\rho_a)$. Vex represents excess adsorption capacity of sample, cm^3/g; V_L is Langmuir volume, cm^3/g; P_L stands for Langmuir pressure, MPa; P stands for equilibrium pressure,

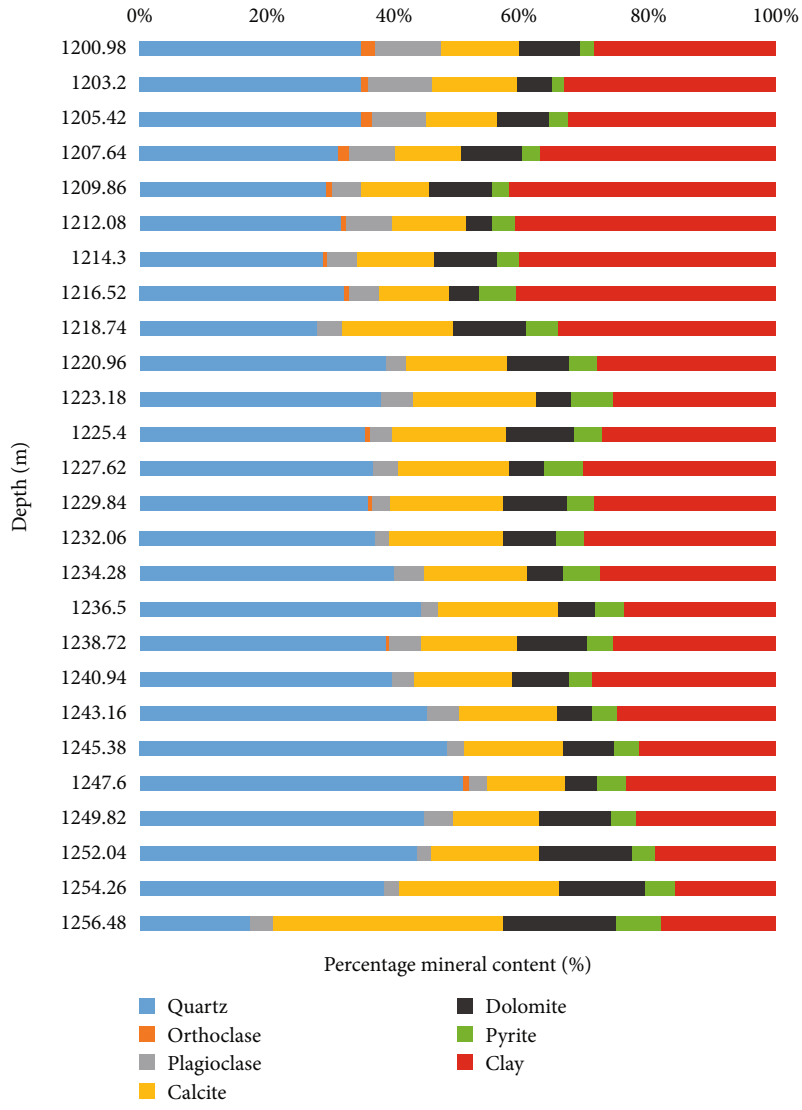

Figure 5: Vertical distribution of LF mineral components in well L4.

MPa; ρ_a represents the adsorption methane density, g/cm^3. ρ_g represents methane gas density at different pressure points, g/cm^3; finally, the isothermal adsorption curve was obtained.

3.8. Measurement of Fluid Saturation Using NMR. The saturation of movable fluids and bound water in 20 shale samples was measured using a RecCore03 low-magnetic-field NMR core analyzer. The relaxation time of fluids in rock pores depends on the intensity of the action of the solid surface imposed on fluid molecules [32]. A strong force between the water molecules and the solid surface indicates a bound fluid and small T2 value; otherwise, movable fluids are indicated [34, 35]. According to the observed intensity and attenuation rule of H_2 NMR signals, the location and the content of the fluids were ascertained through inversion, and the transverse relaxation time T2 was measured using the core analyzers. Then, the saturation was determined based on the T2 distribution.

4. Results

4.1. Geochemical Characteristics of Organic Matter. Based on the data from 105 samples taken from six wells, the TOC of LF shale in the study area was determined to be 0.38%–4.76%, with an average of 2.02%. The content of organic matter is primarily 2%–3% (Figure 3), which is relatively high and has good potential for hydrocarbon generation and offers good conditions for the formation of shale reservoirs. As can be seen from Table 1, Most of the organic matter in the study area is of type II1, followed by type II2, the content of organic matter increases with depth. The maturity of organic matter generally reflects the potential for hydrocarbon generation of source rock. In the study area, the

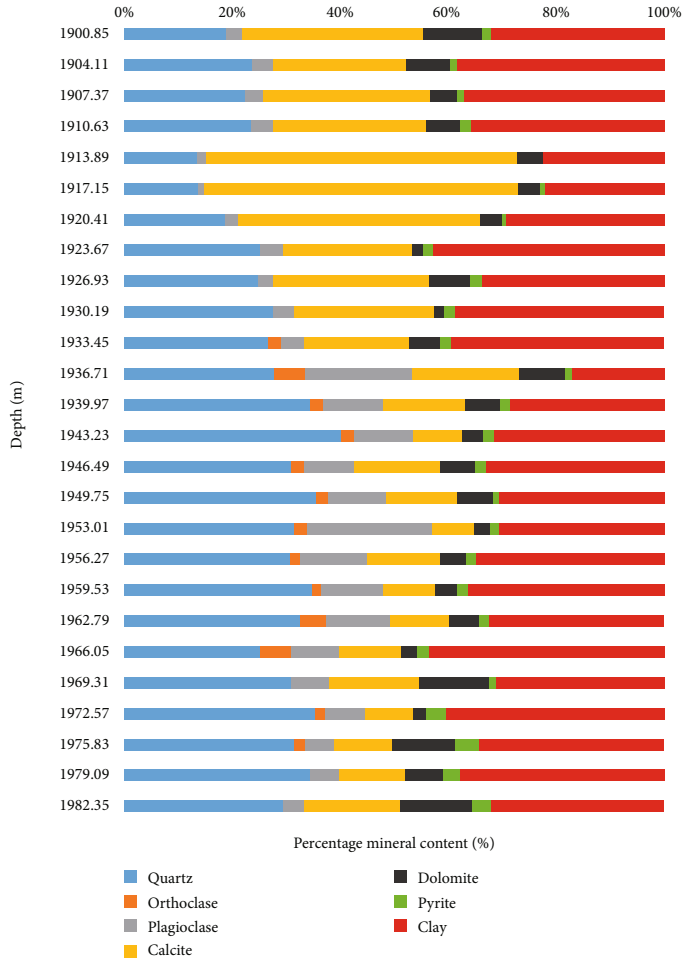

Figure 6: Vertical distribution of LF mineral components in well L7.

maturity of organic matter is 2.02%–2.54%, with an average of 2.23%, indicating that the organic matter is excessively mature, and it mainly produces dry gas. It can be concluded that the shales in the LF has considerable potential for hydrocarbon generation.

4.2. Mineralogical Characteristics

4.2.1. Mineral Components. The mineralogical analysis of 40 samples (Figure 4) shows that the major components include quartz, carbonatite, clay, and a small amount of pyrite. The content of quartz is in the range of 13.6%–42.7%, with an average of 33.5%. The content of pyrite is 0.8%–11.3%, with an average of 3.75%. The content of carbonatite is 19.7%–63.5%, with an average of 32.0%. The content of clay minerals is 15.7%–43.6%, with an average of 30.7%. The clay mineral mainly consists of illite/smectite mixed layers with an average content of 41.5%, illite with an average content of 39.4%, and chlorite with an average content of 18.6%. As can be seen from Figures 5 and 6, as the depth increases, the contents of both quartz and brittle minerals in wells L4 and L7 increase, while the total quantity of clay minerals in the wells decreases (Figure 7). The increased content of brittle minerals indicates that the rocks at deeper domains are more liable to fracture.

Using the SEM images, we studied the relationships between the quartz content and the porosity, between the quartz content and the TOC, and between the TOC and the quartz content. There is a positive correlation between the quartz content and the TOC of well L1 (Figure 8). The positive correlation between the quartz content and the TOC of well L7 is moderate compared to that of well L1, suggesting that the quartz in both wells has a biogenic origin. Since well L1 is relatively far from well L7, it is inferred that there is less terrigenous detrital quartz in the western area where well L1 is situated than in the eastern area where well L7 lies. The feldspar is dominated by plagioclase, followed by minor orthoclase.

4.2.2. Brittleness. Shale brittleness determines the development degree of natural fissures and some pores and thereby affects the content of free gas and the total gas content [36]. Petroleum geologists often use the brittleness index (BI) to represent the fracability and fracturing difficulty of shale [37]. Qualitative and quantitative analyses are generally used to judge the BI of shale. As can be seen in Figures 5 and 6,

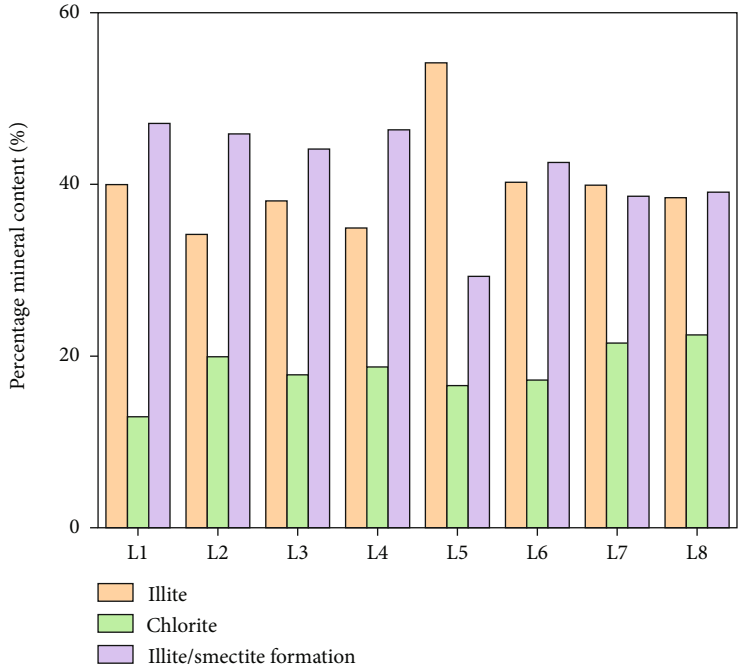

Figure 7: Histogram showing the content distribution of LF clay minerals in wells in the study area.

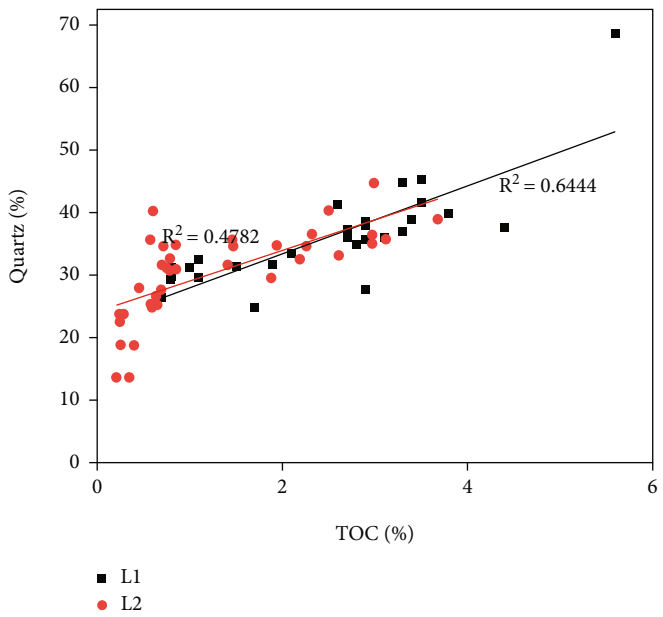

Figure 8: Relationship between the quartz content and the TOC in the LF shale in wells L1 and L7.

when the percentage of brittle minerals in the area increases, the BI also increases. The BI of 56 samples randomly taken from 8 wells was calculated to be 13.9–46.2%, with an average of 37.4%. (BI = (quartz(%)/quartz(%) + clay minerals (%) + carbonatite (%)) ×100% [1];) The shale in the study area has moderate brittleness and the BI of each well slightly differs, indicating that shale has roughly the same brittleness. This information is valuable for the future fracturing-based mining of shale.

4.3. Physical Properties. By analyzing 48 samples from six wells, it was determined that the rocks have very low porosity and permeability. The porosity was determined to be 0.108%–6.202%, with an average of 1.91% (Figure 9), and the permeability was determined to be 0.000172–4.67433 mD (Figure 10), with an average of 0.233019 mD. The permeability is dominated by the range of 0.000–0.01 mD and is extremely high locally because of the presence of microfissures. The porosity-permeability cross-plot

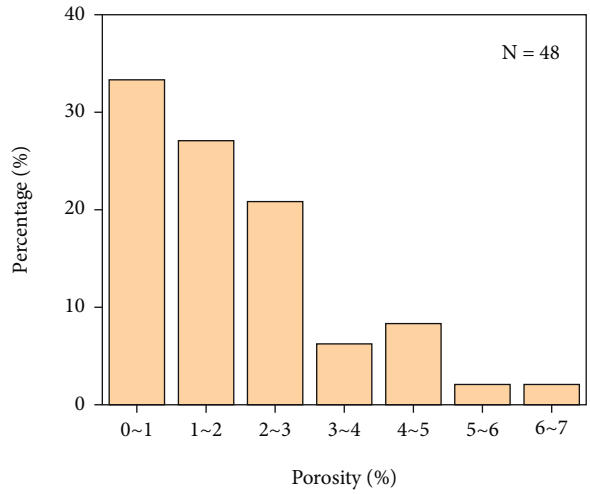

Figure 9: Histogram showing the frequency distribution of porosity.

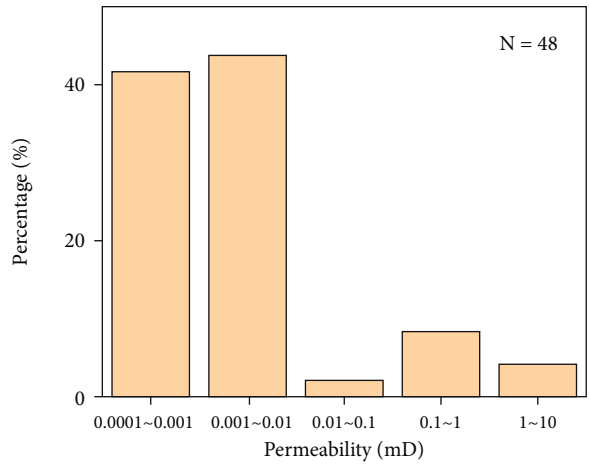

Figure 10: Histogram showing the frequency distribution of permeability.

shows that there is no correlation between these (Figure 11), which is possibly due to the following reasons. (1) There are many organic matter-hosted pores, which is possibly because of the very low permeability induced by the presence of organic matter between pores and the throats. (2) The pore structure parameters are negatively correlated with the content of clay minerals. This is possible because pore throats are filled as a result of clay minerals absorbing water and expanding, leading to abnormal permeability. The low porosity and high permeability may be caused by microfissures. Therefore, it is obvious that the permeability of rocks in shale reservoirs is not controlled by porosity but by the entire pore network.

4.4. Pore Structure. The SEM images show that there are organic matter-hosted pores, intergranular pores, intragranular pores, and microfissures in the shale in the area.

(1) Organic pores

Organic pores are formed when organic matter generates hydrocarbons. They are an important storage space for shale and allow for significant raise in the SSA of the shale pore system. Numerous organic matter-hosted pores can be seen in these samples, as shown in Figure 12(a).

(2) Microfissures

Microfissures serve as primary seepage pathways and the main storage space for free gas in shale reservoirs [38], as shown in Figure 12(b).

(3) Intercrystal pores

Intercrystal pores mainly refer to the pores that form inside the pyrite framboids. Intercrystal pores are common in shale, as shown in Figure 12(c).

(4) Intragranular pores

Intragranular pores mainly develop on the surfaces of carbonatite and quartz, as shown in Figure 12(d). Owing to differences in the physical properties of different minerals, intragranular pores with different genetic mechanisms form. Mineral-corroded pores are common.

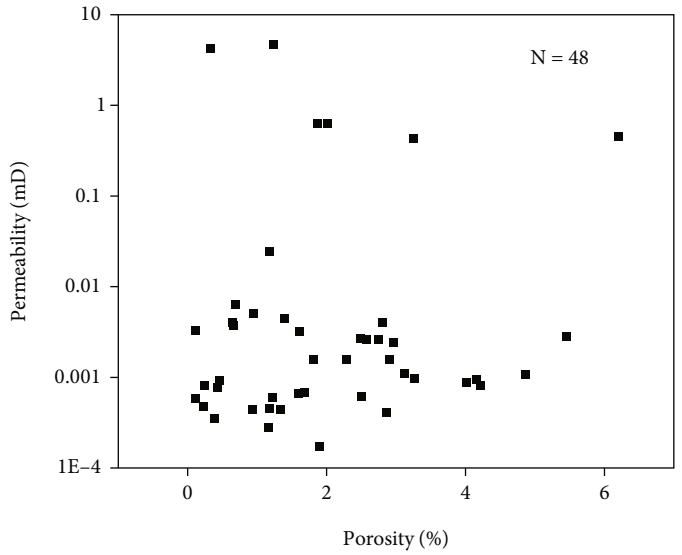

Figure 11: Porosity-permeability cross-plot.

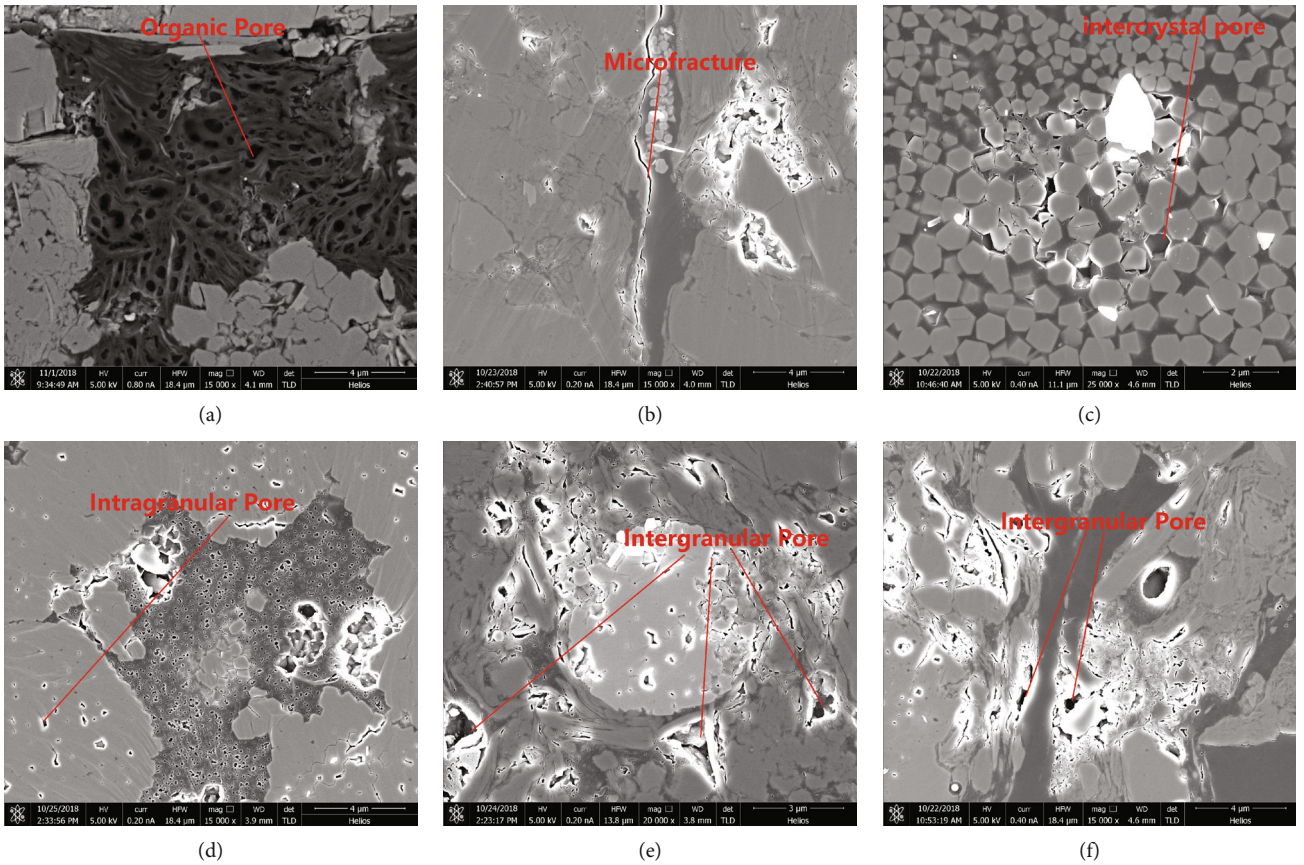

(a) (b) (c)

(d) (e) (f)

Figure 12: Images showing the pore characteristics of LF shale in well L1; (a) well L1, organic matter-hosted pore, LWF, 1057.97 m; (b) well L1, microfissure, LWF, 1069.38 m; (c) well L1, intercrystal pore, LWF, 1081.67 m; (d) well L1, intragranular pore, LWF, 1063.05 m; (e) well L1, intergranular pore, LWF, 1075.33 m; (f) well L1, intergranular pore, LWF,1081.67 m.

Table 2: Pore structure in the study area.

Sample no.	Depth/m	BET specific surface area, m^2/g	BJH total pore volume, cm^3/g	Average pore size/nm
L1-7	1039.45	16.20	0.0248	8.40
L1-14	1057.97	23.00	0.0331	8.40
L1-17	1063.05	23.30	0.0332	8.40
L1-20	1069.38	23.60	0.0324	8.30
L1-23	1075.33	24.40	0.0331	8.30
L2-3	1659.96	20.80	0.0327	9.70
L2-5	1665.68	21.00	0.0326	9.90
L2-7	1668.77	22.10	0.0340	9.70
L2-14	1685.95	27.20	0.0335	8.70
L3-3	1479.25	23.34	0.0328	8.98
L3-8	1489.52	26.26	0.0344	8.67
L3-11	1498.56	27.13	0.0340	8.34
L6-3	2644.71	12.35	0.0208	9.38
L6-5	2649.62	14.00	0.0235	9.62
L6-7	2653.38	13.35	0.0230	9.53
L6-15	2671.59	20.36	0.0297	8.61
L6-21	2683.24	19.69	0.0307	9.30
L7-6	1916.8	8.63	0.0196	11.9

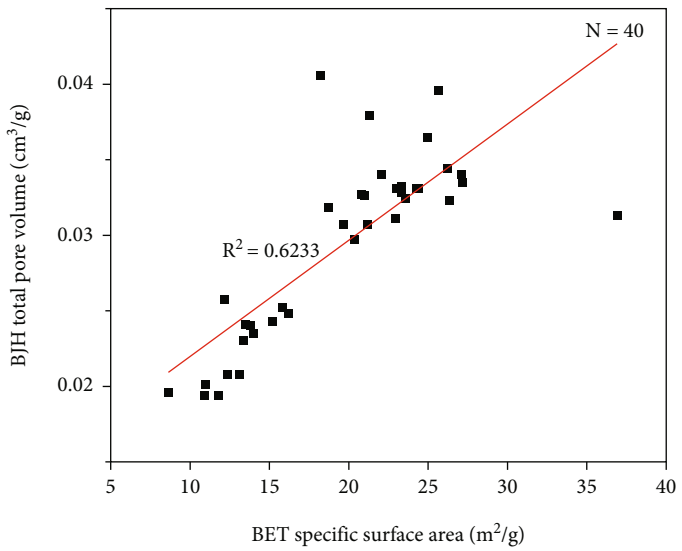

Figure 13: Relationship between the SSA and the total pore volume.

Table 3: Statistics of brittleness index of all wells in the study area.

Sample (number)	Min.	Max.	Average
8	36.72%	44.92%	40.87%
5	35.03%	42.07%	39.27%
7	30.16%	46.21%	41.38%
9	35.18%	44.64%	40.96%
5	29.85%	42.16%	37.43%
7	36.57%	41.26%	38.71%
9	13.91%	41.40%	29.34%
6	22.71%	42.46%	32.73%

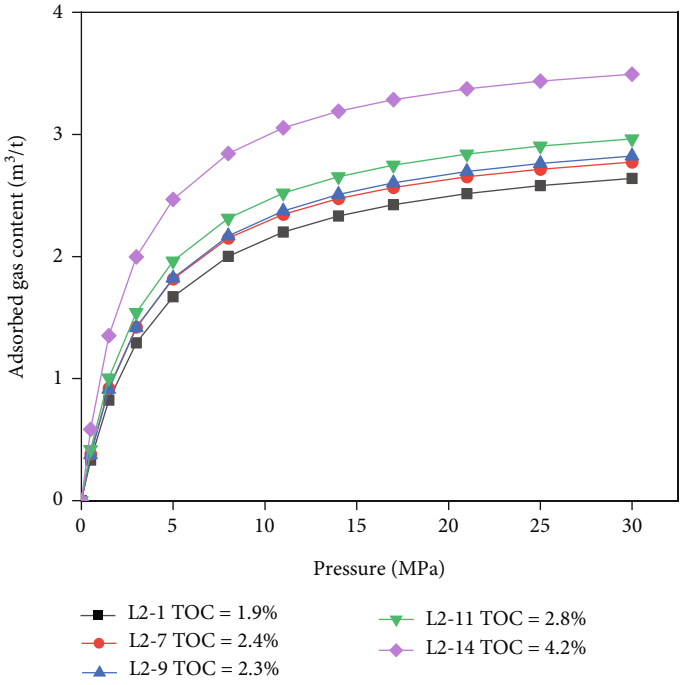

Figure 14: The results from the isothermal adsorption in well L2.

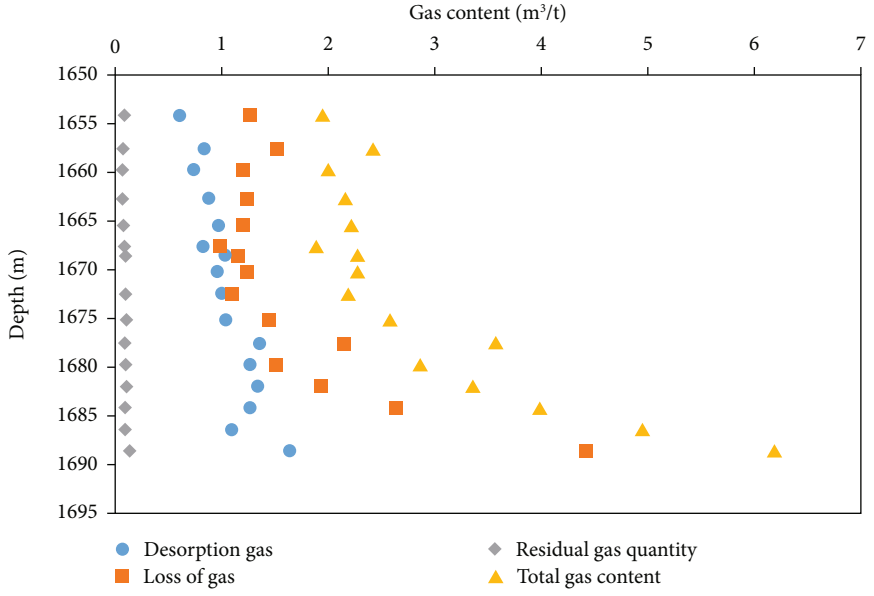

Figure 15: Curves showing vertical variation in the gas content of well L2.

(5) Intergranular pores

Intergranular pores develop among brittle mineral particles or pores that form under the support of brittle minerals, as shown in Figures 12(e) and 12(f).

According to the pore size classification method of the International Union of Pure and Applied Chemistry (IUPAC), pores are divided into three sizes, namely macropores (≥50 nm), mesopores (2–50 nm), and micropores (≤2 nm). Based on data from the low-temperature N2 adsorption experiments of 18 randomly selected samples, the authors calculated that the pore size is 8.3–11.9 nm (average: 9.12 nm) in the shale reservoirs in the study area. Therefore, the pores are mostly mesopores, as shown in Table 2. The total pore volume of the shale reservoirs in the study area

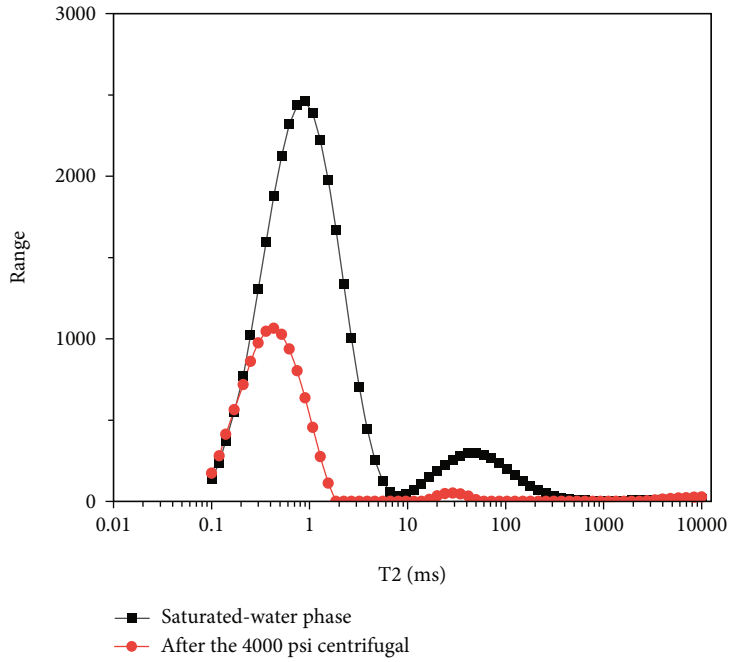

Figure 16: T2 distribution of L1-1 before and after centrifugation.

is closely correlated with the SSA (Figure 13). That is, the SSA increases as the pore volume increases. The BJH total pore volume is 0.019–0.034 cm^3/g, with an average of 0.029 cm^3/g. The BET SSA is 8.63–27.20 m^2/g, with an average of 22.59 m^2/g (Table 3). These parameter values of samples from each well increase with an increase in depth. In general, the pores in shale reservoirs in the study area have a relatively large SSA, which is favorable for shale gas adsorption.

4.5. Gas-Bearing Characteristics

4.5.1. Characteristics of Isothermal Adsorption. Isothermal adsorption experiments were performed on shale samples from well L2. It can be seen from Figure 14 that under isothermal conditions, the absolute adsorbed gas volume rapidly increased in stages 0–10. In the process of gradual pressurization, the increase in absolute adsorbed gas volume began to slow down until it reached a steady state. When the pressure rose from 0 to 8 MPa, the excessive adsorbed gas volume rapidly increases with an increase in pressure, and it began to gradually decrease at 8 MPa. As seen in the figure, data from five samples show that the increase in the TOC corresponds with an increase in the adsorbed gas content. However, the increase in adsorbed gas is closely related to pressure.

4.5.2. Measured Gas Content. Measurements of the gas content of 76 shale samples from five wells demonstrate that the desorbed gas volume is 0.08–1.63 m^3/t, with an average of 0.745 m^3/t, and that the lost gas volume is 0.12–4.41 m^3/t, with an average of 1.221 m^3/t. The high lost gas volume indicates that free gas accounts for a high proportion of the lost gas volume in the area. The residual gas volume is 0.04–0.16 m^3/t, with an average of 0.086 m^3/t. The total gas content is 0.28–6.18 m^3/t, with an average of 2.0534 m^3/t. As shown in Figure 15, the curves reflecting the vertical variation of the gas content in well L2 shows that the gas content and the free gas content in the LF increase with an increase in depth, and the gas content is higher than 0.5 cm^3/g—he lower limit for industrial exploitation of shale gas. Therefore, the LF shale reservoirs have the potential for exploration.

4.6. Measured Water Saturation. Quantifying the saturation of a rock with a movable fluid by the change in water content volume and T2 distribution of the rock before and after centrifugation (full water state before centrifugation, bound water state after centrifugation). The area under the left peak of the NMR curve represents the bound fluid content, while the area under the right peak represents the movable fluid content (Figure 16).

5. Discussion

5.1. Influencing Factors of Pore Characteristics. Pore size and its distribution and pore volume are important for fluid storage and transport in shale [39]. The development of pores in shale reservoirs is affected by many factors, such as the total organic carbon and mineral components in shale [40].

5.1.1. Total Organic Carbon. The TOC is one major factor in hydrocarbon generation and also directly controls the development of organic matter-hosted pores [41]. As can be seen from Figure 17(a), the TOC has a certain positive correlation with the porosity, indicating that organic matter forms organic matter-hosted pores in the process of hydrocarbon generation and thereby affects shale porosity. As shown in

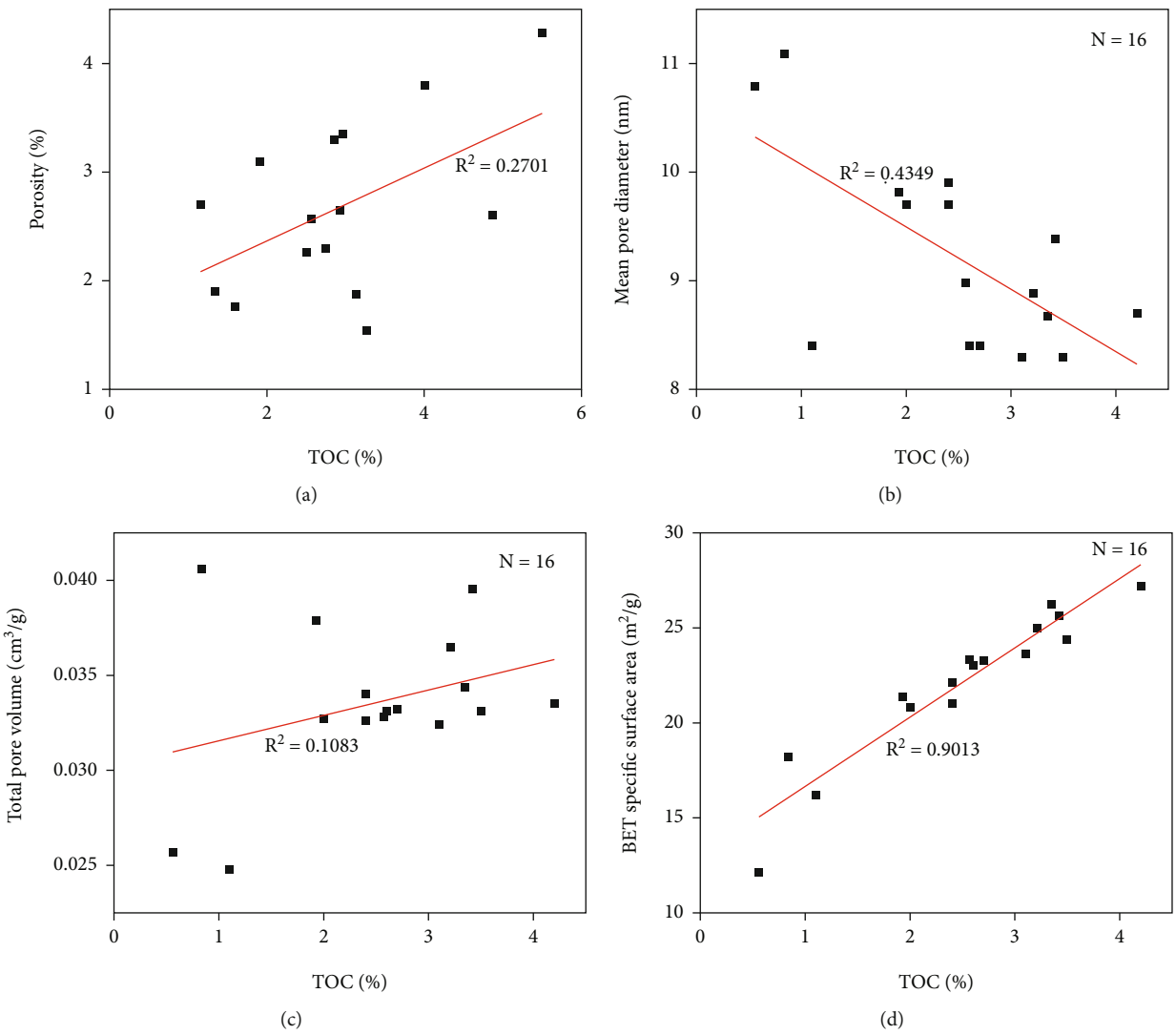

Figure 17: Relationships between the TOC and pore parameters.

Figure 17(b), the TOC has a negative correlation with the average pore size, indicating that organic matter may block pores. As can be seen in Figure 17(c), the TOC has a poor correlation with the total pore volume. As Figure 17(d) demonstrates, the TOC has a close positive correlation with the BET SSA and the total pore volume. Overall, the organic matter-hosted pores developed in the LF shale in the study area are the main contributor to the SSA, but they are not a favorable contributor to the porosity and the total pore volume. The total organic carbon is an important factor influencing the capacity of pores to store natural gas.

5.1.2. Mineral Components. Mineral components affect the development and later transformation of shale reservoirs. The quantitative and qualitative analyses of the mineral components and pore structure of shale samples were conducted by scanning whole rocks with SEM and XRD. The analytical results reveal that the shale in the study area is mainly composed of organic clay minerals, quartz, and feldspar and that the pore characteristics are affected by organic matter, quartz, and clay. The SSA of clay minerals generally increases with an increase in their contents, and different clay minerals show different SSAs. As can be seen from the clay mineral composition in Figure 6, the clay minerals in the study area mainly include illite and illite/smectite mixed layers, which have limited SSA according to previous studies [42]. Consequently, the contribution of illite and illite/smectite to the SSA of shale in the study area is not apparent. The following inferences are drawn from the data presented in this study. (1) The quartz content in the shale in the study area has a strong correlation with TOC, while there is a moderate correlation between TOC and porosity. It can be seen from Figures 18(a) and 18(b) that the quartz content has a moderate influence on the porosity and SSA of the shale. As shown in Figures 18(c) and 18(d), the quartz content is poorly correlated with the total pore volume and negatively correlated with the average pore size. Apart from the fact that the quartz itself has few pores, the possible

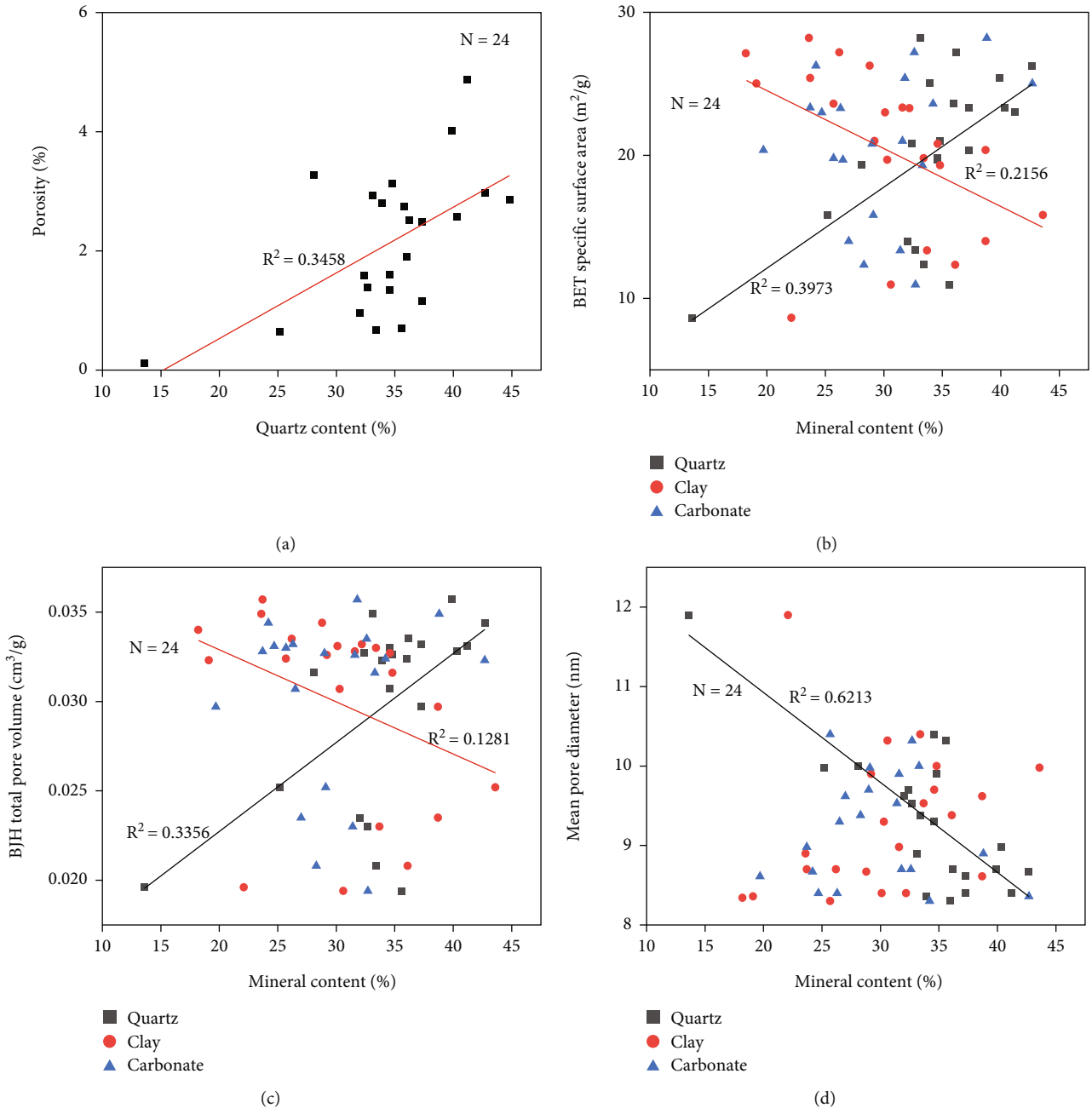

Figure 18: Relationships between different minerals and pore parameters.

reason is that pores are blocked due to the collapse of minerals such as quartz under physical and chemical actions. (2) As Figure 18(b) shows, there is a negative correlation between the content of clay minerals and the SSA. As a result, it is inferred that some pore throats may be blocked by clay particles. It is also possible that this negative correlation is caused by the negative correlation between the TOC and clay minerals (Figure 19). However, there is a positive correlation between the TOC and SSA. Therefore, it can be inferred that TOC may conceal the impacts of clay minerals on the SSA of shale.

5.2. Influencing Factors of Gas Content

5.2.1. Total Organic Carbon and Maturity. As can be seen from Figure 20(a), the total gas content and the desorbed gas volume has a strong positive correlation with the TOC. Meanwhile, numerous nanolevel pores are generated in the process of thermal evolution. Both contribute to higher SSA for the adsorption of methane gas [43]. The isothermal adsorption curves in Figure 14 show that the volume of adsorbed gas in shale gradually increases with an increase in the TOC. This indicates that the TOC significantly

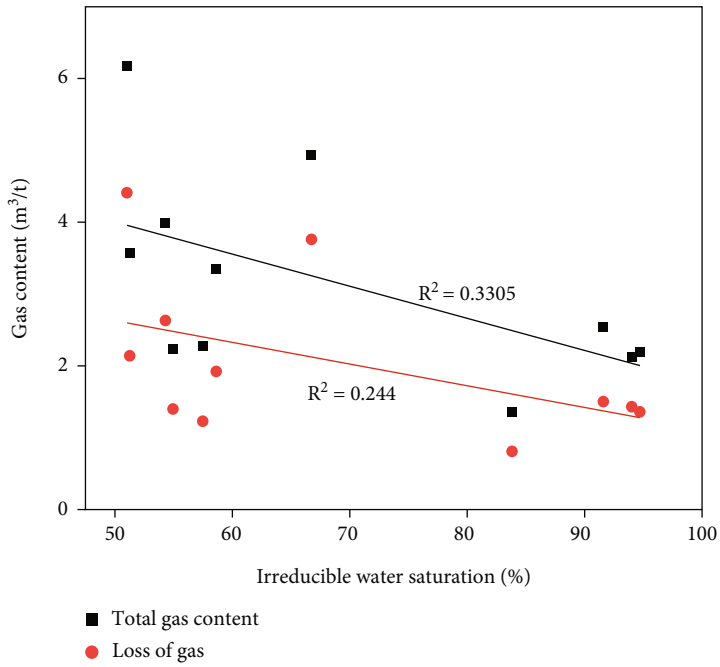

Figure 19: Relationships between the bound water saturation and the gas content.

influences the content of gas in the LF in the study area and that the TOC has a positive correlation with porosity (Figure 17(a)). The LF in the study area contains developed organic matter-hosted pores, which are vital places for gas adsorption and contribute significantly to the SSA and the total pore volume (Figure 17(d)). Therefore, the TOC plays an important role in the gas content.

5.2.2. Mineral Components. As shown in Figures 20(b) and 20(c), there is a certain positive correlation between the quartz content and the gas content, indicating that many pores were formed by the interactions between quartz grains and organic carbon and that many microfissures were formed by the fragmentation of quartz particles. As a result, quartz grains contain a large amount of natural gas. The BI and the gas content increase with an increase in depth, which is mainly due to the following two reasons. (1) The BI is important to the contents of brittle minerals and to the primary intergranular pores of brittle minerals; and (2) the broken brittle particles generate various pores, causing the shale gas storage spaces to rise. Figure 20(c) shows the negative correlation between the content of clay minerals and the content of the desorbed gas, which is inconsistent with previous study results [44, 45]. Analysis of the correlation between the TOC and clay minerals shows that the TOC has a strong negative correlation with the content of clay minerals (Figure 19) and a positive correlation with the surface area. Since the SSA serves as a vital space for natural gas storage, clay minerals have a negative impact on the pore's SSA. As a result, there is a negative correlation between the desorbed gas volume and the content of clay minerals. Figure 20(c)shows that there is a negative correlation between the clay content and the total gas content. Theoretically, the total gas content increases with the increase of clay minerals, but the figure shows a negative correlation. The main reason may be that the influence of clay minerals on gas content is overwritten by the influence of TOC because of the negative correlation between clay minerals and TOC. In addition, the possible reason is that the clay particles blocked the pores, resulting in reduced storage space of free gas or that the clay minerals adsorbed water and expanded, resulting in reduced total pore volume and reduced total gas content.

5.2.3. Pore Characteristics. The positive correlation between the SSA and the desorbed gas volume in shale and between the total pore volume and the desorbed gas volume indicates that the desorbed gas originates from the adsorbed gas in the micropores. High SSA allows more shale gas to be absorbed, thus affecting the desorbed gas volume. Since pores provide storage spaces for shale gas, the total pore volume affects the gas content.

5.2.4. Water Saturation. As can be seen from Figure 21, higher bound water saturation in shale pores indicates a larger pore space occupied by water, a larger proportion of free gas in the study area, and a smaller space available for gas. Therefore, the bound water saturation has an adverse effect on the free gas volume. Meanwhile, the clay minerals in shale expand in the presence of water, and the pore surface available for shale gas adsorption decreases in the case of a certain internal surface of pores. Therefore, higher water content indicates a smaller area available for shale gas adsorption and less absorbed gas. Finally, a negative

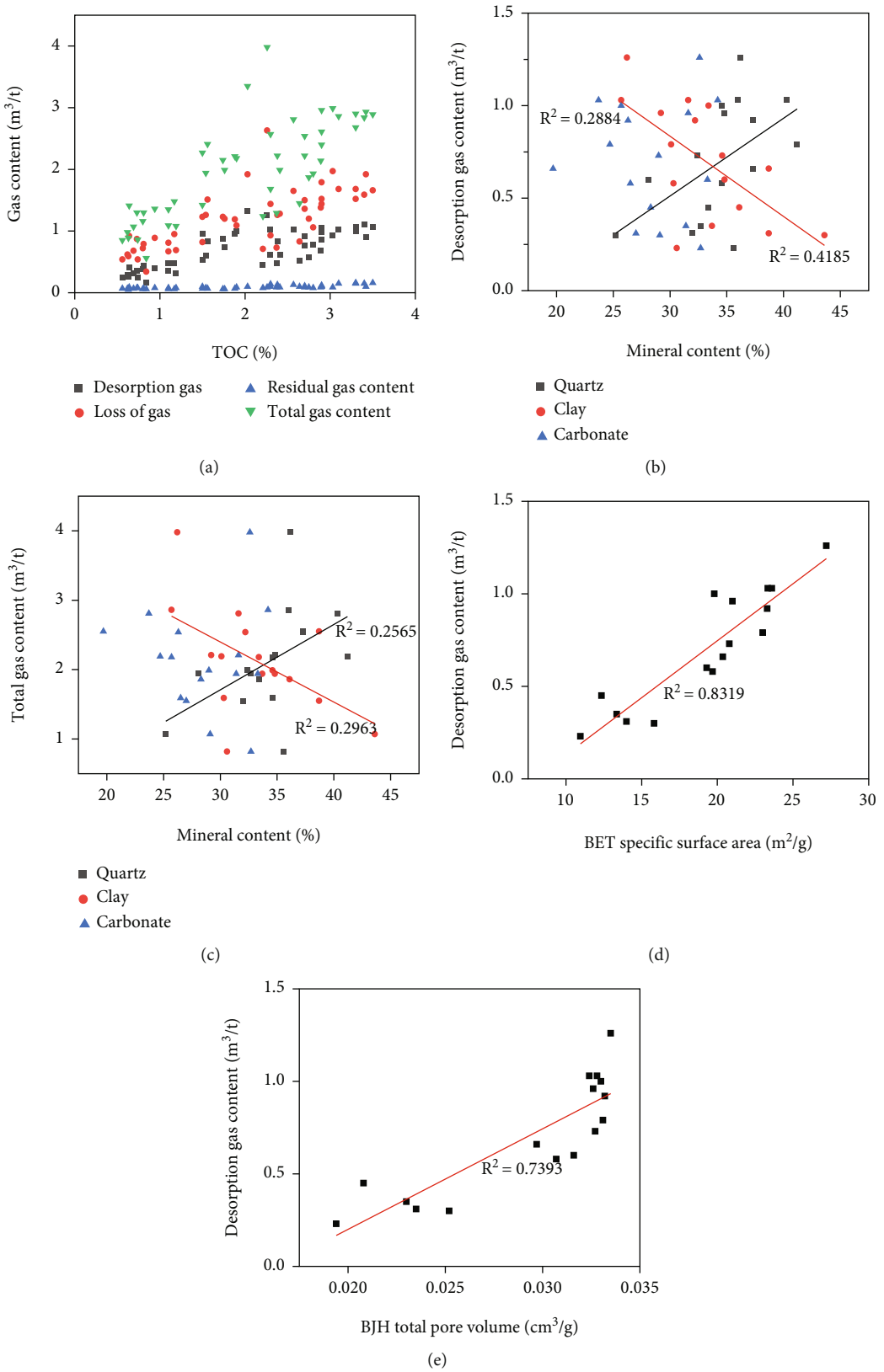

Figure 20: Relationships between influencing factors of gas-bearing properties of shale samples.

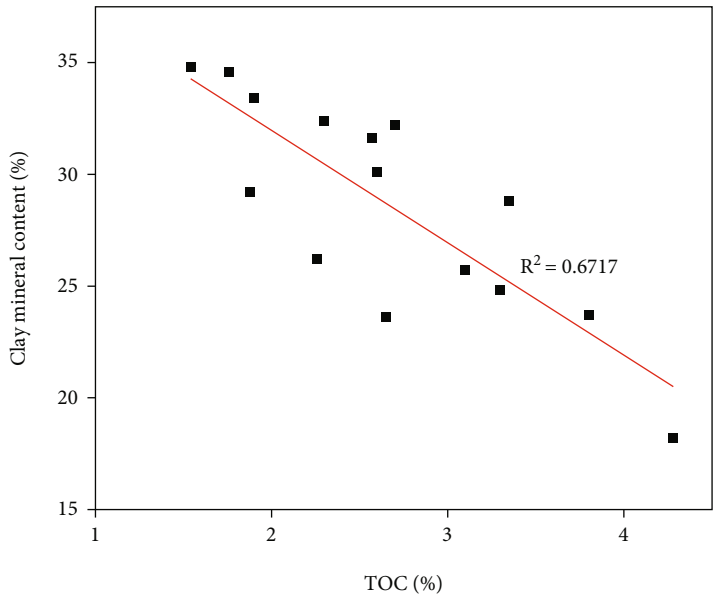

Figure 21: Relationship between clay mineral content and the TOC.

correlation between the total gas content and the bound water saturation is formed.

6. Conclusions

Our study on the shale reservoirs from LF leads to the following conclusions.

(1) The rocks have high TOC (average: 2.02%) and high maturity of organic matter (average: 2.23%). These are favorable conditions for organic matter. The LF has moderate brittleness, which increases with an increase in depth, and the average BI is 37.4%. There are several types of pores, mainly including organic matter-hosted pores, intergranular pores, intragranular pores, and microfissures, most of which are mesopores with an average pore size of 9.12 nm. The total gas content of the LF also increases with increasing depth, with an average of 2.05 m^3/t. Therefore, the study area has good potential for shale gas exploitation

(2) The pore structure is affected by the organic matter content and mineral components in the study area. As a result, organic matter-hosted pores have primarily developed. The porosity and SSA are positively correlated with the TOC, whereas clay minerals have an adverse effect on the pore SSA

(3) The gas content in the study area is affected by the organic matter content, pore maturity, mineral components, pore characteristics, and water saturation. Higher TOC and Ro indicate higher gas content. As the depth increases, both the contents of brittle minerals and gas content increase. It can be inferred that the particles of brittle minerals break and form storage spaces of shale gas. Higher SSA and higher total pore volume indicate greater adsorbed gas volume. The bound water saturation of rocks has an adverse effect on the content of desorbed gas

Data Availability

The figures and tables used to support the findings of this study are included in the article.

Conflicts of Interest

The authors declare that there are no conflicts of interest regarding the publication of this paper.

Acknowledgments

The authors would like to extend their gratitude to the Natural Science Foundation of Xinjiang Uygur Autonomous Region (Grant No. 2020D01C037), The National Natural Science Foundation of China (Grant No. 42062010), and Tianshan Innovation Team Program (2020D14023).

References

[1] J. B. Curtis, "Fractured shale-gas systems," *AAPG Bulletin*, vol. 86, no. 11, pp. 1921–1938, 2002.

[2] D. M. Jarvie, R. J. Hill, T. E. Ruble, and R. M. Pollastro, "Unconventional shale-gas systems: the Mississippian Barnett Shale of north-central Texas as one model for thermogenic shale-gas assessment," *AAPG Bulletin*, vol. 91, no. 4, pp. 475–499, 2007.

[3] J. Li, X. B. Wang, L. H. Hou et al., "Geochemical characteristics and resource potential of shale gas in Sichuan Basin, China," *Journal of Natural Gas Geoscience*, vol. 6, no. 8, pp. 313–327, 2021.

[4] M. N. Ge, F. Pang, and S. J. Bao, "Micro pore characteristics of Wufeng-Longmaxi shale and their control on gas content: a

case study of well Anye 1 in Zunyi area, Guizhou Province," *Petroleum Geology & Experiment*, vol. 41, no. 1, pp. 23–30, 2019.

[5] Z. J. Jin and M. S. Yuan, "Reservoiring mechanism of shale gas and its distribution," *Natural Gas Industry*, vol. 24, no. 7, pp. 15–18, 2004.

[6] C. N. Zou, Z. Yang, G. S. Zhang et al., "Concepts, characteristics, potential and technology of unconventional hydrocarbons: on unconventional petroleum geology," *Petroleum Exploration and Development*, vol. 40, no. 4, pp. 413–428, 2013.

[7] Y. Chen, C. Jiang, J. Y. Leung, A. K. Wojtanowicz, and D. Zhang, "Multiscale characterization of shale pore-fracture system: geological controls on gas transport and pore size classification in shale reservoirs," *Journal of Petroleum Science and Engineering*, vol. 202, article 108442, 2021.

[8] C. Z. Jia, "Breakthrough and significance of unconventional oil and gas to classical petroleum geology theory," *Petroleum Exploration and Development*, vol. 44, no. 1, pp. 1–10, 2017.

[9] C. N. Zou, Q. Zhao, G. S. Zhang, and B. Xiong, "Energy revolution: from a fossil energy era to a new energy era," *Natural Gas Industry*, vol. 3, no. 1, pp. 1–11, 2016.

[10] S. A. Solarin, L. Gil-Alana, and C. Lafuente, "An investigation of long range reliance on shale oil and shale gas production in the U.S. market," *Energy*, vol. 195, article 116933, 2020.

[11] R. Weijermars, N. Sorek, D. Sen, and W. B. Ayers, "Eagle Ford Shale play economics: U.S. versus Mexico," *Journal of Natural Gas Science and Engineering*, vol. 38, pp. 345–372, 2017.

[12] D. Z. Dong, Y. M. Wang, X. J. Li et al., "Breakthrough and prospect of shale gas exploration and development in China," *Natural Gas Industry*, vol. 3, no. 1, pp. 12–26, 2016.

[13] D. Z. Dong, Q. L. Guo, Y. Song et al., "Establishment and practice of unconventional oil and gas geology," *Acta Petrolei Sinica*, vol. 93, no. 1, pp. 12–23, 2019.

[14] G. Y. Zhai, Y. F. Wang, S. J. Bao et al., "Major factors controlling the accumulation and high productivity of marine shale gas and prospect forecast in southern China," *Earth Science*, vol. 42, no. 7, pp. 1057–1068, 2017.

[15] D. Z. Dong, S. K. Gao, J. L. Huang, Q. Z. Guan, S. F. Wang, and Y. M. Wang, "A discussion on the shale gas exploration & development prospect in the Sichuan Basin," *Natural Gas Industry*, vol. 34, no. 12e, pp. 1–15, 2014.

[16] D. Z. Dong, Z. S. Shi, Q. Z. Guang et al., "Progress, challenges and prospects of shale gas exploration in the Wufeng- Longmaxi reservoirs in the Sichuan Basin," *Natural Gas Industry*, vol. 5, no. 5, pp. 415–424, 2018.

[17] X. H. Ma and J. Xie, "The progress and prospects of shale gas exploration and development in southern Sichuan Basin, SW China," *Petroleum Exploration and Development*, vol. 45, no. 1, pp. 172–182, 2018.

[18] F. Wang, J. Liu, and J. Zhang, "Early postnatal noise exposure degrades the stimulus-specific adaptation of neurons in the rat auditory cortex in adulthood," *Neuroscience*, vol. 404, no. 15, pp. 1–13, 2019.

[19] J. Z. Yi, H. Y. Bao, A. W. Zheng et al., "Main factors controlling marine shale gas enrichment and high-yield wells in South China: a case study of the Fuling shale gas field," *Marine and Petroleum Geology*, vol. 103, pp. 114–125, 2019.

[20] J. H. Zhao, Z. J. Jin, Q. H. Hu et al., "Geological controls on the accumulation of shale gas: a case study of the early Cambrian shale in the Upper Yangtze area," *Marine and Petroleum Geology*, vol. 107, pp. 423–437, 2019.

[21] D. Z. Ren, L. T. Ma, D. K. Liu, J. Tao, X. Q. Liu, and R. J. Zhang, "Control mechanism and parameter simulation of oil-water properties on spontaneous imbibition efficiency of tight sandstone reservoir," *Frontiers in Physics*, vol. 10, article 829763, 2022.

[22] M. E. Curtis, B. J. Cardott, C. H. Sondergeld, and C. S. Rai, "Development of organic porosity in the Woodford Shale with increasing thermal maturity," *International Journal of Coal Geology*, vol. 103, pp. 26–31, 2012.

[23] O. Iqbal, E. Padmanabhan, A. Mandal, and J. Dvorkin, "Characterization of geochemical properties and factors controlling the pore structure development of shale gas reservoirs," *Journal of Petroleum Science and Engineering*, vol. 206, article 109001, 2021.

[24] D. K. Liu, D. Z. Ren, K. Du, Y. R. Qi, and F. Ye, "Impacts of mineral composition and pore structure on spontaneous imbibition in tight sandstone," *Journal of Petroleum Science and Engineering*, vol. 201, article 108397, 2021.

[25] D. Z. Ren, H. P. Zhang, Z. Z. Wang, B. Y. Ge, D. K. Liu, and R. J. Zhang, "Experimental study on microscale simulation of oil accumulation in sandstone reservoir," *Frontiers in Physics*, vol. 176, no. 10, article 841989, 2022.

[26] N. N. Liu, "Micro pore structure characteristics of high quality shale section of Longmaxi formation in Nanchuan area," *Petroleum Geology and Engineering*, vol. 35, no. 4, pp. 21–25, 2021.

[27] A. Q. Jia, D. F. Hu, S. He et al., "Variations of pore structure in organic-rich shales with different lithofacies from the Jiangdong block, Fuling shale gas field, SW China: insights into gas storage and pore evolution," *Energy and fuels*, vol. 34, no. 10, pp. 12457–12475, 2020.

[28] K. L. Xi, Y. C. Cao, B. G. Haile et al., "How does the pore-throat size control the reservoir quality and oiliness of tight sandstones? The case of the Lower Cretaceous Quantou Formation in the southern Songliao Basin, China," *Marine and Petroleum Geology*, vol. 76, no. 1-15, pp. 1–15, 2016.

[29] F. Zhang, Z. X. Jiang, W. Sun et al., "A multiscale comprehensive study on pore structure of tight sandstone reservoir realized by nuclear magnetic resonance, high pressure mercury injection and constant-rate mercury injection penetration test," *Marine and Petroleum Geology*, vol. 109, pp. 208–222, 2019.

[30] G. C. Jing, Z. X. Chen, and G. Hui, "A novel model to determine gas content in naturally fractured shale," *Fuel*, vol. 306, article 121714, 2021.

[31] Z. Li, J. C. Zhang, D. J. Gong et al., "Gas-bearing property of the Lower Cambrian Niutitang Formation shale and its influencing factors: a case study from the Cengong block, northern Guizhou Province, South China," *Marine and Petroleum Geology*, vol. 120, article 104556, 2020.

[32] Y. S. Pan, Z. L. Huang, X. B. Guo, B. C. Liu, G. Q. Wang, and X. F. Xu, "Study on the pore structure, fluid mobility, and oiliness of the lacustrine organic-rich shale affected by volcanic ash from the Permian Lucaogou Formation in the Santanghu Basin, Northwest China," *Journal of Petroleum Science and Engineering*, vol. 208, article 109351, 2022.

[33] J. Q. Li, S. F. Lu, P. F. Zhang et al., "Estimation of gas-in-place content in coal and shale reservoirs: a process analysis method and its preliminary application," *Fuel*, vol. 259, article 116266, 2020.

[34] J. Q. Li, S. Wang, S. Lu et al., "Microdistribution and mobility of water in gas shale: a theoretical and experimental study," *Marine and Petroleum Geology*, vol. 102, pp. 496–507, 2019.

[35] X. H. Shao, X. Q. Pang, H. Li et al., "Pore network characteristics of lacustrine shales in the Dongpu Depression, Bohai Bay Basin, China, with implications for oil retention," *Marine and Petroleum Geology*, vol. 96, pp. 457–473, 2018.

[36] F. B. Miao, Z. Q. Peng, Z. X. Wang, B. M. Zhang, C. S. Wang, and L. Gong, "Brittleness characteristics and influencing factors of marine shale of Niutitang Formation in Xuefeng region: a case study of Well XZD-1," *Geology in China*, pp. 1–18, 2021.

[37] Y. M. Wang, D. Z. Dong, J. Z. Li et al., "Reservoir characteristics of shale gas in Longmaxi Formation of the Lower Silurian, southern Sichuan," *Acta Petrolei Sinica*, vol. 33, no. 4, pp. 551–561, 2012.

[38] R. Y. Ma, J. Zhang, M. Wang, W. P. Ma, and J. G. Zhao, "Micro-pore characteristics and gas-bearing properties of marine continental transitional shale reservoirs in the Qinshui basin," *Journal of Henan Polytechnic University (Natural Science)*, vol. 40, no. 4, pp. 66–77, 2021.

[39] C. Z. Xu, *Research on Shale Reservoir Characteristic of Wufeng Lower Longmaxi Formation in Dianqianbei Depression*, Xinjiang University, 2020.

[40] S. G. Liu, K. Jiao, J. C. Zhang et al., "Research progress on the pore characteristics of deep shale gas reservoirs: an example from the Lower Paleozoic marine shale in the Sichuan Basin," *Natural Gas Industry*, vol. 41, no. 1, pp. 29–41, 2021.

[41] K. Ke, J. H. Qin, B. X. Mou et al., "Properties and main influences of mud shale reservoir in the Baiguowan Formation, Xichang Basin," *Acta Sedimentologica Sinica*, pp. 1–18, 2021.

[42] S. Ning, "Study on Wufeng Formation-Longmaxi Formation organic matter rich shale pore features in Fenggang workspace no.1- a case study of well XX," *Coal Geology of China*, vol. 33, no. 7, pp. 27–33, 2021.

[43] L. Ji, J. Qiu, and Y. Xia, "Micro-pore characteristics and methane adsorption properties of common clay minerals by electron microscope scanning," *Acta Petrologica Sinica*, vol. 33, no. 2, pp. 249–256, 2012.

[44] K. L. Wang, K. Q. Li, L. K. Wang, H. L. Gao, K. W. Li, and P. Q. Hu, "Mineral composition and gas-bearing characteristics of shale from Wufeng-Longmaxi Formation in Shizhu area, eastern margin of Sichuan Basin," *Journal of Lanzhou University(-Natural Sciences)*, vol. 54, no. 3, pp. 285–291, 2018.

[45] J. Xia, S. B. Wang, T. T. Cao, J. Z. Yang, and Z. G. Song, "The characteristics of pore structure and its gas storage capability of the lower Cambrian shales from northern Guizhou Province," *Natural Gas Geoscience*, vol. 26, no. 9, pp. 1744–1754, 2015.